Synthesis, Characterization, Biological and *in silico* ADMET Studies of Mixed Ligand Transition Metal Complexes Based on Novel Schiff Base and 1,10-Phenanthroline

S. Syed Ali Fathima[1,*,] and M. Mohamed Sahul Meeran[2,]

[1]International Research Centre, Department of Chemistry, Kalasalingam Academy of Research and Education, Krishnankoil-626126, India
[2]Jana Marine Service Co. Limited, Al Khobar, Kingdom of Saudi Arabia

*Corresponding author: E-mail: syed.s@klu.ac.in

The main objective of this work is to mitigate the challenges associated with the use of platinum-based chemotherapy drugs through investigating chemotherapeutic compounds based on mixed ligand transition metal complexes. Thus, Cu(II), Co(II), Ni(II) and Zn(II) complexes were synthesized from novel Schiff base compound derived from 2-amino-3-hydroxypyridine and 5-chloro-2-nitrobenzaldehyde and the co-ligand 1,10-phenanthroline. The spectral investigations were conducted to characterize the synthesized compounds and revealed that they possess an octahedral structure. The interactions of synthesized compounds with calf thymus DNA (*ct*-DNA) demonstrated that the binding takes place through an intercalation. Comparatively to Schiff base ligand, the synthesized transition metal complexes proved to be better anti-pathogenic agent when tested against bacteria. The prepared compounds possess more the biological capability, according to *in silico* ADMET study, which may attributed to the presence of two N-heterocyclic ligands. The computational screening of biological activities related to cancer activity using PASS software propose the drug-like nature of the compounds.

Keywords: Mixed ligand complexes, Schiff base, 1,10-Phenanthroline, DNA, Anticancer potential, ADMET.

INTRODUCTION

Cytotoxic drugs based on platinum make up most of the drugs used to treat cancer. The potential of heavy metal complexes in cancer treatment is significant, although their toxicity limits their practical use [1-5]. Consequently, chemotherapeutic research has shifted its focus to the non-platinum based compounds that would make ideal substitutes due to the increasing demand for novel anticancer therapies with lower toxicity. Since copper is an endogenous metal, it is believed that its complexes will exhibit lesser toxicity than those of platinum compounds. For this reason, several transition metal compounds have garnered particular attention [6,7].

The use of pyridine based drugs in clinical medicine has expanded to address a wider range of conditions. The pharmacological activities exhibited by pyridine based drugs include antihypertensive, anticoagulant, antihistaminic, antibacterial, anti-inflammatory, antifungal, antiviral, antitubercular, antidiabetic and antimalarial effects [8,9]. Some pyridine based drugs can directly inhibit membranes at high concentrations, without depending on sterols and sterol esters.

The chemistry of coordination of mixed ligands containing transition and non-transition metal ions is crucial for the functioning of metalloenzymes and other biological processes [10,11]. Metal complexes generally have greater bioactivities compared to free ligands. Furthermore, complexation can help mitigate certain side effects and reduce medicine tolerance. A mixed ligand complex is differentiated from a conventional complex by the inclusion of two or more distinctive ligand types that are attached to a single metal ion inside the complex [12].

Therefore, we report herein the synthesis of mixed ligand metal(II) complexes from 2-amino-3-hydroxy-pyridine, 5-chloro-2-nitrobenzaldehyde and 1,10-phenanthroline (co-ligand), which coordinated with transition metals Cu(II), Co(II), Ni(II) and Zn(II). 1,10-Phenanthroline was chosen as a co-ligand because it is an electron-conjugated heterocyclic aromatic ligand with a stronger coordinating capacity due to its N-donor chelation nature, which forms stable complexes. The synthesized mixed ligand complexes were found to bind to DNA efficiently and might potentially be turned into DNA probes. Furthermore, the data for their cytotoxicity and antibacterial activity sugge-

sted that they are suitable for development as potent cytotoxic, antimicrobial and therapeutic drugs.

EXPERIMENTAL

The chemicals employed in this study were of AnalaR grade and used without additional purification. However, solvents were used as purified solvents by distillation method. The chemicals 2-amino-3-hydroxypyridine and 5-chloro-2-nitro-benzaldehyde, 1,10-phenanthroline, calf-thymus DNA and ethidium bromide were acquired from Sigma-Aldrich, USA. Merck Chemicals Ltd., India provided ethanol, DMSO and metal(II) salts.

The elemental analysis was carried out in Perkin-Elmer-240 elemental analyzer instrument. The molar conductivity of the complexes in DMSO (10^{-3} M) solvent was measured at room temperature using deep vision 601 model digital conductivity meter. The vibration spectral data were obtained by using FT-IR Shimadzu model IR-Affinity-1 spectrophotometer using KBr discs. Similarly, the electronic spectra were measured using Shimadzu UV Vis-1800 spectrometer at room temperature. ^{1}H NMR and ^{13}C NMR spectral data were recorded by using Bruker 300 MHz Advance III HD Nanobay NMR spectrometer with DMSO-d_6 as a deuterated solvent. The mass spectra were performed by using JEOL-AccuTOF JMS-T100LC mass spectrometer equipped with a custom-made electro spray interface (ESI). The X-band of the EPR spectrum was recorded by JES-FA 200 spectrometer at liquid nitrogen temperature (LNT) (77 K) and room temperature (300 K). EDAX spectral data of the complexes were performed by AMETEK-EDAX (Analyzer). The SEM and colour mapping images were retrieved from the instrument model ZE ISS EVO 18 Research instrument. The powder XRD was taken using Shimatzu XRD-6000 X-ray diffractometer with 2θ ranges from 10-80° and the surface morphology was studied by a field emission scanning electron microscopy (FESEM) (Model SUPRA 40) with a voltage of 30 KV. The absorption spectra were recorded using UV-visible spectrophotometer (Shimadzu model UV-1601) at room temperature for DNA binding studies. The anticancer activity of newly synthesized compounds was evaluated against a couple of cancer cell lines and normal cell lines by MTT assay.

Synthesis of Schiff base ligand: The Schiff base ligand was synthesized by condensing 40 mL of hot ethanolic solution of 5-chloro-2-nitrobenzaldehyde (1 g, 10 mmol) with 30 mL of hot ethanolic solution of 2-amino-3-hydroxypyridine (10 mmol) containing few drops of glacial acetic acid. The solution was allowed to stirred continously for 3 h at room temperature (**Scheme-I**). After filtration, the precipitate was recrystallized

with ethanol and dried *in vacco*. Colour: dark yellow, yield: 88%. Elemental analysis of $C_{12}H_8N_3O_3Cl$; calcd. (found) %: C, 51.91 (50.91); H, 2.90 (2.87); N, 15.13 (15.05); Cl, 12.77 (15.05); FT-IR (KBr disc, v_{max}, cm^{-1}): 3546 (-OH), 1675 (-CH=N); ^{1}H NMR (DMSO-d_6) δ ppm: 7.30-8.27 (m), (-CH=N) 9.30 (s); (-OH) 9.87 (s); ^{13}C NMR (DMSO-d_6) δ ppm: 120-135.08 (m), (-CH=N) 152.38 (s), (C-OH) 159.07 (s), ESI-MS: 277.66.

Synthesis of mixed ligand metal complexes: The Schiff base ligand (5.54 g, 20 mmol), corresponding metal(II) chloride salt (10 mmol) and co-ligand 1,10-phenanthroline (1.80 g, 10 mmol) were mixed in ethanol (2:1:1). After 8 h of sonication, the resultant mixture was allowed to reflux for 24 h and ethanol was used to wash the resulting product before it was recrystallized again (**Scheme-II**). The crystalline solid was vacuum dried on anhy-drous CaCl$_2$.
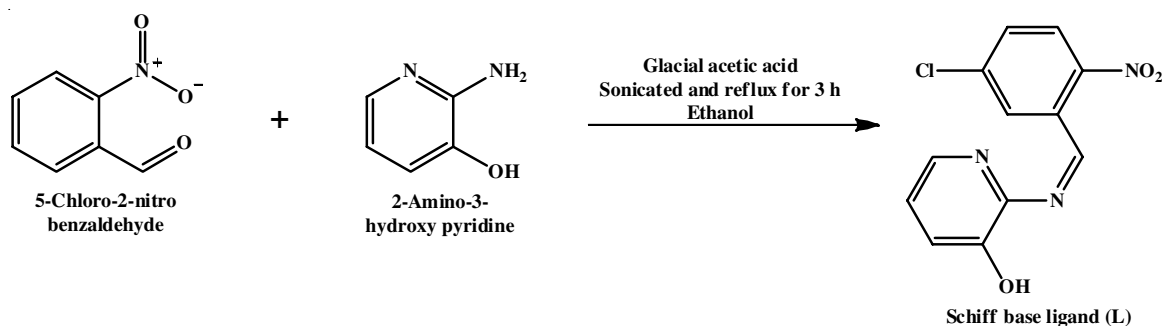
Copper complex: Colour: brown; yield: 83%; Elemental anal. of $C_{36}H_{22}Cl_2CuN_8O_6$ (m.w.: 797); calcd. (found) %: C, 54.25 (53.12); H, 2.78 (2.65); N, 14.06 (13.95); Cu, 12.04 (12.01); $\Lambda_m \times 10^{-3}$ (Ω^{-1} mol^{-1} cm^{-2}) 14; μ_{eff}: 1.77 B.M.; λ_{max} (nm) in DMSO 605 (*d-d*); FT-IR (KBr, v_{max}, cm^{-1}): 1692 (-CH=N); 534 (M-O), 433 (M-N); ESI-MS: 798.12 (M+1) *m/z*.

Cobalt complex: Colour: dark brown; yield: 82%; Elemental anal. of $C_{36}H_{22}Cl_2CoN_8O_6$ (m.w.: 792); calcd. (found) %: C, 54.56 (54.34); H, 2.80 (2.75); N, 14.14 (14.06); Co, 7.44 (7.44); $\Lambda_m \times 10^{-3}$ (Ω^{-1} mol^{-1} cm^{-2}) 16; μ_{eff}: 1.98 B.M.; λ_{max} (nm) in DMSO 642 (*d-d*); FT-IR (KBr, v_{max}, cm^{-1}): 1690 (-CH=N); 524 (M-O), 434 (M-N).
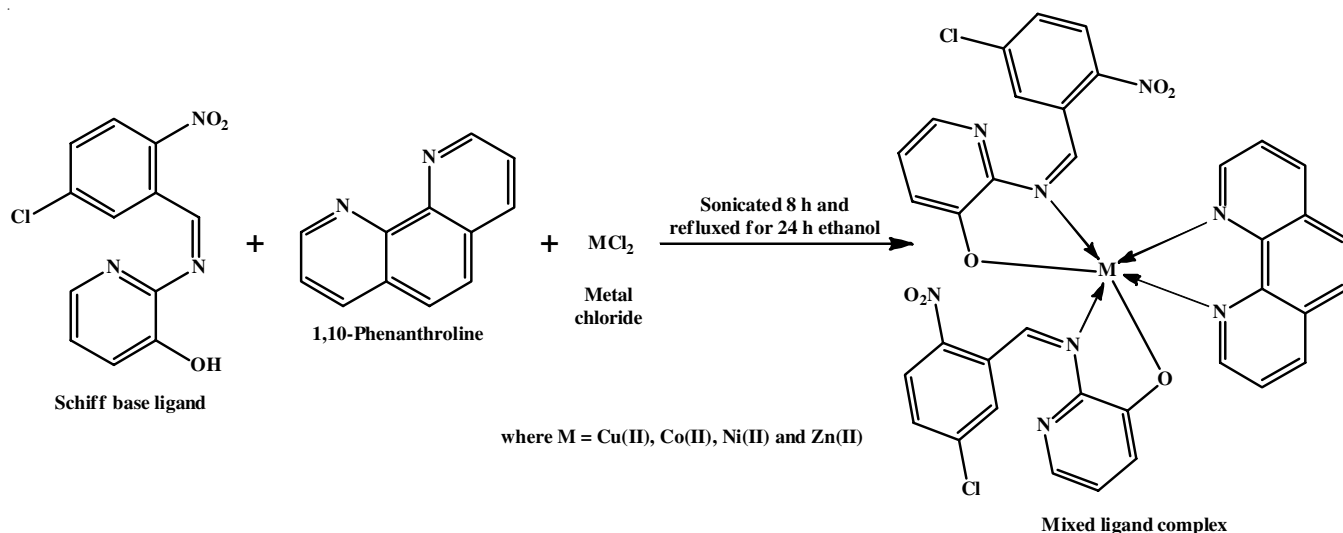
Nickel complex: Colour: dark green, yield: 86%; Elemental anal. of $C_{36}H_{22}Cl_2NiN_8O_6$ (m.w.: 792); calcd. (found) %: C, 54.58 (54.44); H, 2.80 (2.77); N, 14.14 (14.11); Ni, 7.41 (7.21); $\Lambda_m \times 10^{-3}$ (Ω^{-1} mol^{-1} cm^{-2}) 17; μ_{eff}: 3.27 B.M.; λ_{max} (nm) in DMSO 635 (*d-d*); FT-IR (KBr, v_{max}, cm^{-1}): 1592 (-CH=N), 548 (M-O), 432 (M-N).

Zinc complex: Colour: pale green, yield: 79 %; ; Elemental anal. of $C_{36}H_{22}Cl_2ZnN_8O_6$ (m.w.: 798); calcd. (found) %: C, 54.12 (53.24); H, 2.78 (2.72); N, 14.03 (13.95); Zn, 8.18 (8.17); $\Lambda_m \times 10^{-3}$ (Ω^{-1} mol^{-1} cm^{-2}) 16; μ_{eff}: diamagnetic; λ_{max} (nm) in DMSO 323 (LMCT); FT-IR (KBr, v_{max}, cm^{-1}): 1596 (-CH=N), 539 (M-O), 431 (M-N); ^{1}H NMR (DMSO-d_6) δ ppm: 6.91-8.55 (m, aromatic H), 9.14 (s, -CH=N); ^{13}C NMR (DMSO-d_6) δ ppm: 120.00-135.08 (m, aromatic-C), 161.18 (s, -CH=N), 169.28 (s, C=O).

DNA binding experiments: At room temperature, the metal complexes were allowed to interact with *ct*-DNA in a Tris-HCl buffer (5 mM Tris-HCl/50 mM NaCl) medium with 5% DMSO (pH 7.2). The absorption spectra were recorded

5-Chloro-2-nitro benzaldehyde

2-Amino-3-hydroxy pyridine

Glacial acetic acid Sonicated and reflux for 3 h Ethanol

Schiff base ligand (L)

Scheme-I: Synthesis of Schiff base ligand

Scheme-II: Synthesis of mixed ligand complex

using a Shimadzu model UV-1601 spectrophotometer. Prior to and after DNA addition, the spectra of metal complexes were recorded using buffer solution to dilute the concentrated stock solution of synthesized compounds (10^{-3} M) to the appropriate concentrations for each experiment [13]. To conduct these absorption spectrum titrations, nucleic acid was added to the complex solution at a constant concentration. The titration method was repeated until the absorption values become constant, indicating that the saturation of binding sites [14].

Viscosity measurements: Ostwald viscometer was used to measure viscosity at a controlled temperature of 30.0 ± 0.1 ºC in a thermostat water-bath. The difficulties caused by the flexibility of *ct*-DNA were minimized by sonicating a 0.5 mmol sample of *ct*-DNA [15]. The digital stopwatch was used three times to measure the flow time for each complex and then an average flow time was determined. The data were calculated against η/η_o and the concentration of synthesized compounds, where η and η_o is the viscosity of *ct*-DNA with metal complexes and without metal complexes, respectively. The viscosity value of the metal(II) complexes were measured after calculating the flow time of buffer alone (t_o) using the formula $\eta = (t - t_o)/t_o$ [16].

DNA damage studies: The extent of pBR 322 DNA cleavage was monitored by agarose gel electrophoresis in the presence of an activator H_2O_2 as an oxidizing agent [17]. In this reaction super coiled pBR322 plasmid DNA Form I (1 µg) in DMSO (1%, 2 µL) was treated with synthesized compounds (250 µg) and oxidizing agent H_2O_2 (40 mmol, 5 µL). The samples were incubated at 1 h at 310 K. A loading of buffer containing bromophenol blue (0.25%), glycerol (30%) and xylene cyanol (0.25%) was added to a platform fixed with a comb to form slots. The electrophoresis was performed at 50 V for 1 h in tris-boric acid-EDTA) buffer using 1% agarose gel containing 0.5 µg/mL ethidium bromide. The effectiveness of the synthesized compounds was measured by determining the capability of the complexes converting the supercoiled form of DNA to circular form and finally linear form. An image of the bands was taken using ultraviolet light to visualize it [18].

Antimicrobial assay: The minimum inhibitory concentration (MIC) value of ligand and its metal(II) complexes were tested against bacterial strains (*Staphylococcus aureus*, *Bacillus subtilis* (Gram-positive), *Pseudomonas aeruginosa*, *Klebsiella pneumoniae*, *Salmonella typhi* (Gram-negative) and the fungal strains namely *Aspergillus niger*, *Aspergillus flavus*, *Curvularia lunata*, *Rhizoctonia bataticola*, *Candida albicans*) through a broth dilutions method with the standard antibacterial streptomycin and nystatin, respectively. The test concentration synthesized compounds were prepared from 0.01 to 2.5 mg/mL in the sterile walls of the microtiter plates and using 50 µL of sterile nutrient broth. The MIC values were determined by reading each well at 492 nm in an automated micro plate reader [19,20].

Cytotoxic activity (MTT assay): The *in vitro* cytotoxicity of the synthesized compounds against cancer cell lines including human breast adenocarcinoma (MCF-7) and human liver cancer cells (Hep G2) as well as non-cancerous cell lines such as HBL-100, which were obtained from the National Centre for Cell Science (NCCS) in Pune, India, was assessed using the MTT (3-(4,5-dimethyl thiazol-2yl)-2,5-diphenyl tetrazolium bromide) assay. The cell lines were cultured in Dulbecco's Modified Eagles Medium (DMEM) (Himedia, India) supplemented with 10% fetal bovine serum (FBS) and 1% antibiotic-antimycotic solutions. All the compounds were produced in cell culture grade DMSO (Himedia). In brief, the cells were seeded in 96-well plates and kept in CO for 24 h for incubation, then treated with different complexes dissolved in DMSO for 24 h. After incubation, the culture medium was removed and 15 mL of MTT was discarded and DMSO (100 mL/well) was added to dissolve the purple formazan product [21]. The experiment was carried out in triplicates and the medium without compounds served as control. The absorbance was measured calorimetrically at 570 nm using an ELISA microplate reader. The percentage of cell viability was calculated using the following formula:

$$IC_{50} = \frac{OD \text{ value of treated cells}}{OD \text{ value of untreated cells (control)}} \times 100$$

Antioxidant assay: The radical scavenging activity of the synthesized compounds was determined by using DPPH assay. The reduction in the absorption of DPPH solution after the addition of an antioxidant was measured and vitamin C (10 mg/mL DMSO) was used as reference. In brief, the freshly prepared DPPH (2.96 mL, 0.1 mM) was added to the different volumes of Schiff base ligand and its mixed ligand metal(II) complexes. After 20 min of dark incubation at room temperature with 3 mL of DPPH as a control, the reaction mixture's absorbance was measured at 517 nm. The percentage of radical scavenging activity of the synthesized compounds were calculated using the following formula:

$$\text{Radical scavenging activity (\%)} = \frac{\text{Abs. control} - \text{Abs. sample}}{\text{Abs. control}}$$

where RSA is the radical scavenging activity; Abs. control is the absorbance of DPPH radical + ethanol; Abs. sample is the absorbance of DPPH radical and synthesized compounds [22].

Computational studies

PASS-biological activity prediction: PASS is one of the online software and it is frequently used in the drug innovation and development environment. This online web tool is used to predict 3678 type of pharmacological effects based on the structure and it interprets the biological active spectra using the 2D structure of the molecule.

***In silico* ADME-Tox property:** In present study, absorption, distribution, metabolism, excretion and toxicity (ADMET) properties of the synthesized compounds were calculated by SwissADME and AdmetSAR online softwares. The priority of optimizing ADME-Tox properties of potential drug molecules was extensively identified. The SMILEY notation of the compound was introduced into the online software to predict the drug likeness score and toxicity [23-25].

RESULTS AND DISCUSSION

The stoichiometric ratios of mixed ligand transition metal complexes (ligand:metal:co-ligand) were found to be 2:1:1, as determined according to the elemental analysis data. In compared to the mixed ligand metal(II) complexes, which are soluble in organic solvents such as DMSO and DMF, the Schiff base is soluble in ethanol. The synthesized mixed ligands metal(II) complexes are non-electrolytic in nature as indicated by their low conductance values.

Electronic spectral studies: Two prominent bands are apparent in free Schiff base ligand at 300 and 310 nm, which represented the $\pi \rightarrow \pi^*$ and $n \rightarrow \pi^*$ transitions, respectively [26]. In all the metal(II) complexes, these transitions are changed to a higher or lower frequency due to ligand coordination with metal ions (Fig. 1). The copper(II) complex exhibits a *d-d* band at 605 nm, which is associated with the $^2E_g \rightarrow ^2T_{2g}$ transition. This *d-d* transition at 642 nm revealed the distorted octahedral geometry of Cu(II) complex and caused by $^4T_{1g}(F) \rightarrow ^4T_{2g}(F)$ transition. The magnetic susceptibility value of 4.23 B.M. provided further evidence for this geometry.
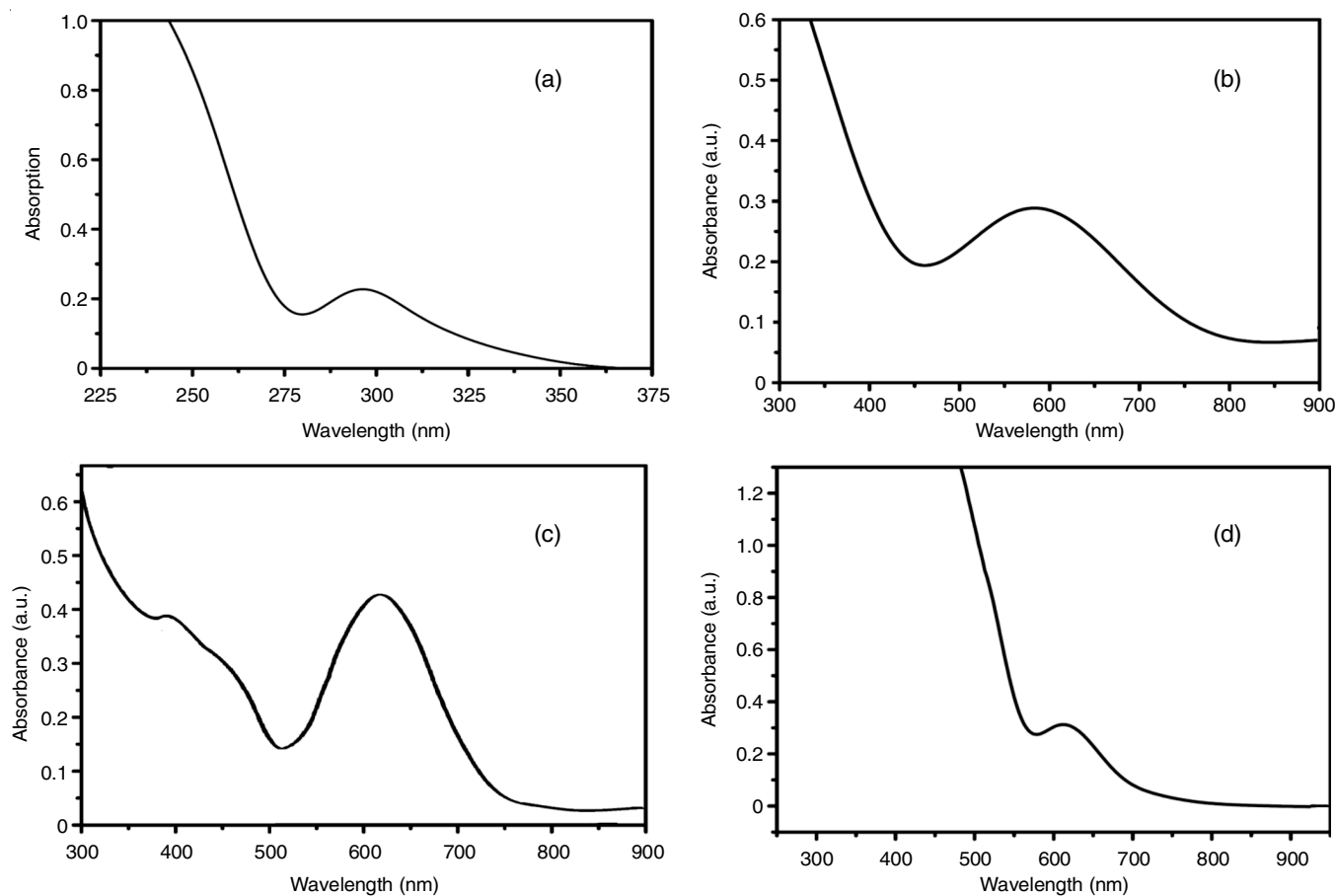

Fig. 1. Electronic spectrum of (a) Schiff base ligand, (b) Cu(II) complex, (c) Ni(II) complex and (d) Co(II) complex

The Ni(II) complex exhibits a *d-d* band at 635 nm corresponds to the $^3A_{2g}(F) \rightarrow {}^3T_{1g}(F)$ transition and revealed the octahedral geometry and is further supported by a magnetic moment value of 3.27 B.M. [27]. The zinc complex, on the other hand, displayed an intra-ligand charge transition (INCT) band due to the absence of *d-d* bands because of fulfilled d^{10} configurations.

FT-IR spectral studies: The spectrum of Schiff base ligand coordinated was quite different from those of metal(II) complexes containing mixed ligands. A broad band in the 3546 cm^{-1} region of Schiff base (Fig. 2a) is attributed due to the ν(OH) group. This band disappeared in the mixed ligand metal(II) complexes (Figs. 2b and 2c), which indicated the deprotonation of the hydroxyl group and coordination with the metal ion [28,29]. However, the azomethine group vibration was linked to the strong band at 1675 cm^{-1} in Schiff base ligand [30]. This band is shifted by 17-22 cm^{-1} in all mixed ligand metal(II) complexes indicating that the metal ion and the nitrogen atom in azomethine are coordinated [31,32]. Moreover, the appearance of two peaks in the lower frequency range of 440-420 cm^{-1} and 540-520 cm^{-1}, are attributed to the ν(M-N) and ν(M-O) vibrations, respectively. These vibrations suggested that the oxygen atom of pyridine (-OH) group and the nitrogen atom of azomethine group of 1,10-phenanthroline moiety (co-ligand) are coordinated with the central metal ion.

NMR spectral studies: Fig. 3 shows the ^1H NMR spectra of Schiff base ligand and Zn(II) complex. Due to the presence of an azomethine proton (-CH=N-) in the synthesized Schiff base, a singlet was detected at δ 9.30 ppm [33,34]. However, this -CH=N- peak moved to δ 8.73 ppm in the Zn(II) complex suggested that azomethine nitrogen participated in the coordination. Further evidence of the deprotonation of -OH group during complexation was provided by the ligand at δ 9.87 ppm, which is caused by the hydroxyl (-OH) proton that vanished in the formed complex [35].

The ^{13}C NMR spectra of the ligand and the Zn(II) complex (Fig. 4) exhibited peaks for aromatic carbons at δ 120.00-135.08 ppm. The signals in Zn(II) complex are moved, which were previously at 161.18 ppm and 169.28 ppm for the –CH=N and -C-OH groups, respectively, up field to 152.38 ppm and 159.07 ppm and the other peaks were unchanged significantly. Therefore, the complexation is confirmed by the changes in peak positions for the –CH=N and –C–OH carbons in the generated complex compared to the ligand [36].

ESI-MS spectral studies: The ESI-MS pattern of free Schiff ligand and Cu(II) compound fragmentation is displayed in Fig. 5. The molecular weight of the Schiff base ligand with the formula $[C_{12}H_8ClN_3O_3]$ and the peak emerged at *m/z* 277.66. Fragmented peaks for the ligand, resulting from the fragmentation of $[C_{12}H_8ClN_3O_2]^+$, $[C_{12}H_9ClN_2]^+$, $[C_{12}H_{10}N_2]^+$, $[C_9H_{10}N_2]^+$, $[C_6H_6N_2]^+$ and $[C_5H_5N]^+$ appeared at *m/z* values of 261.12, 216.13, 182.22, 146.08, 106.05, and 79.04, respectively.

The copper complex exhibited a peak at *m/z* 798.12 correspond to the $[C_{36}H_{22}Cl_2CuN_8O_6]$ species and are comparable to the molecular weight of Cu(II) complex. The fragmentation peaks (*m/z*) appeared at 616.85, 571.86, 537.41, 434.56, 383.51,
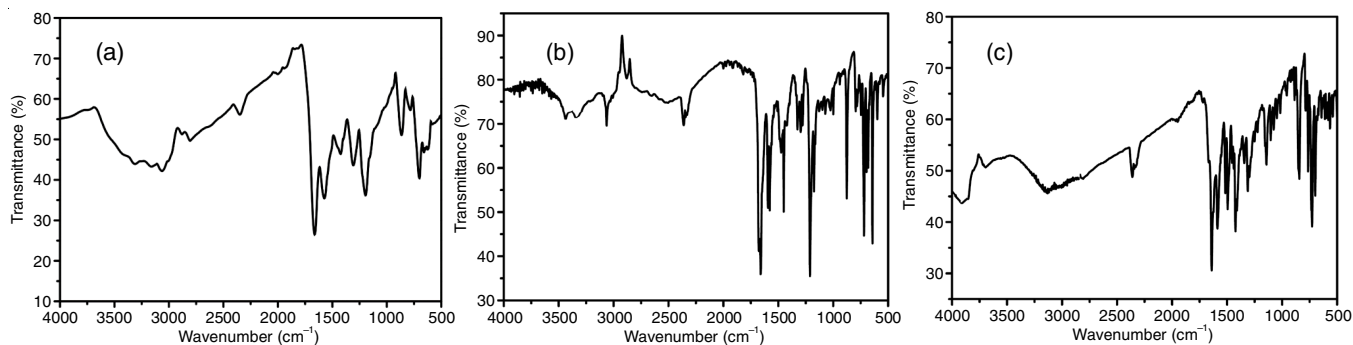

Fig. 2. FT-IR spectrum of (a) Schiff base ligand, (b) Cu(II) metal complex and (c) Ni(II) metal complex
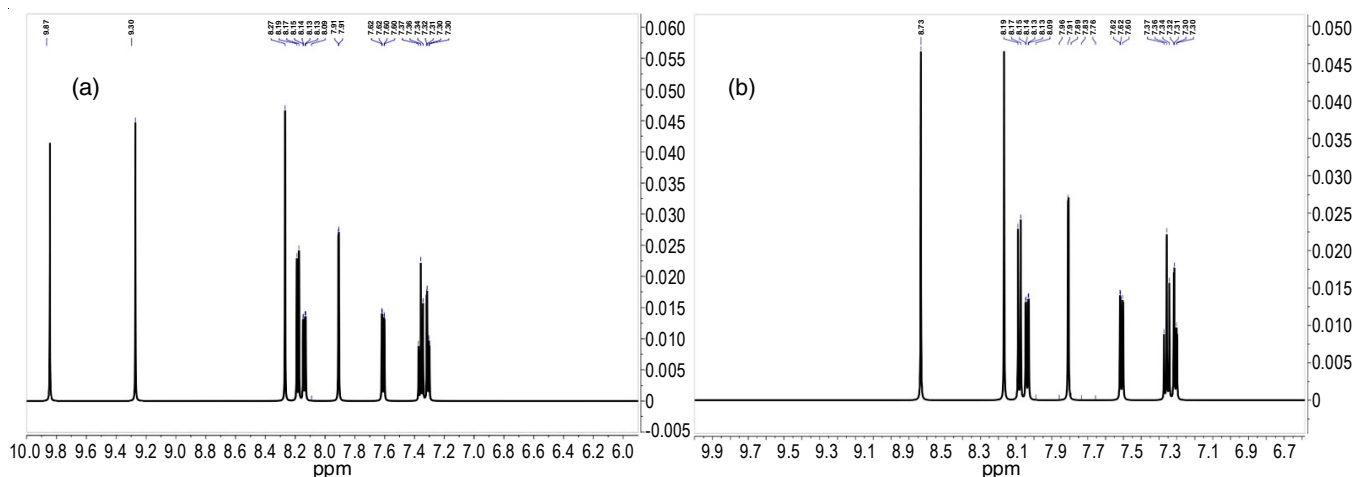

Fig. 3. ^{1}H NMR spectrum of (a) Schiff base ligand and (b) Zn(II) complex
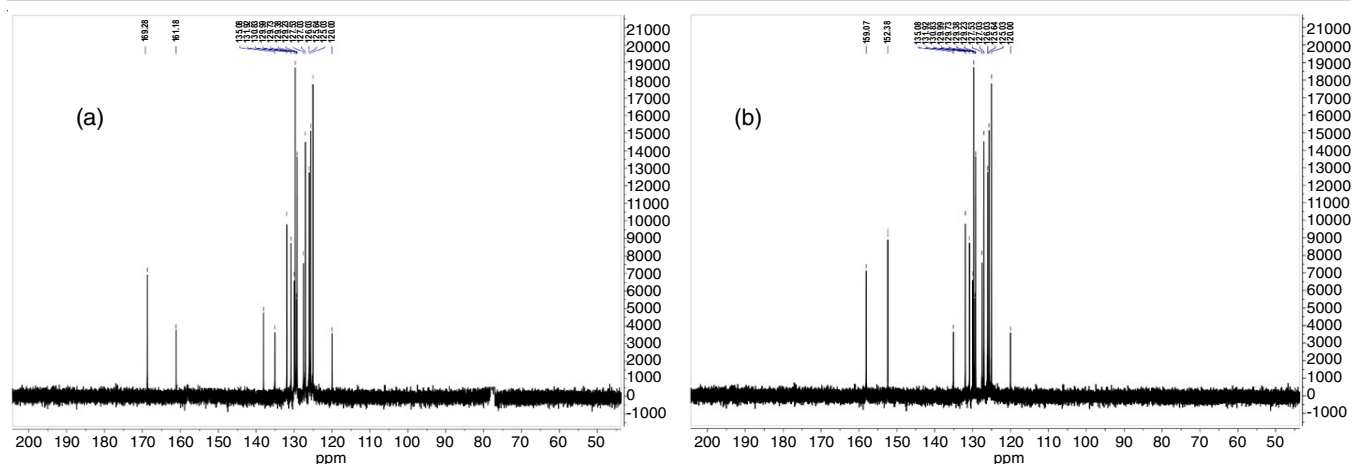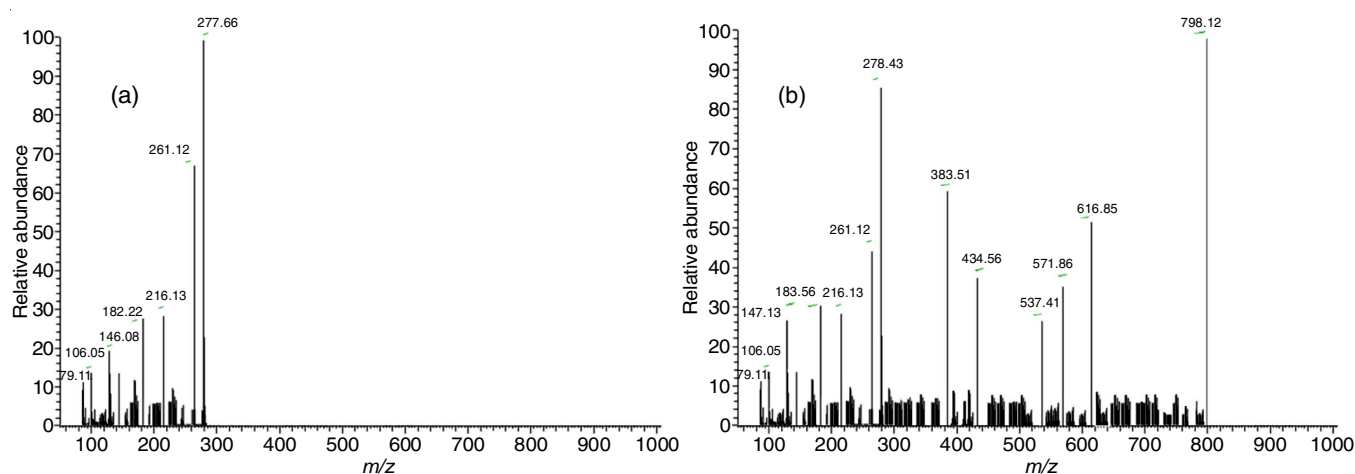
Fig. 4. ^{13}C NMR spectrum of (a) Schiff base ligand and (b) Zn(II) complex

Fig. 5. ESI-MS spectrum of (a) Schiff base ligand and (b) Cu(II) complex

278.43, 261.12, 216.13, 183.56, 147.13, 106.05 and 79.11 correspond to the fragments $[C_{24}H_{14}Cl_2CuN_6O_6]^+$, $[C_{24}H_{15}Cl_2CuN_5O_4]^+$, $[C_{24}H_{16}ClCuN_4O_4]^+$, $[C_{17}H_{11}ClCuN_4O_4]^+$, $[C_{14}H_{10}CuN_3O_4]^+$, $[C_{12}H_8ClN_3O_3]$, $[C_{12}H_8ClN_3O_2]^+$, $[C_{12}H_9ClN_2]^+$, $[C_{12}H_{10}N_2]^+$, $[C_9H_{10}N_2]^+$, $[C_6H_6N_2]^+$ and $[C_5H_5N]^+$, respectively. The observed fragmented peaks supported that the metal complexes were of [ML$_2$(phen)] type, consistent with other spectral observations.

ESR spectral studies: The EPR spectra of the synthesized metal complexes exhibited a characteristic four-line pattern, indicative of their monomeric nature. The spin Hamiltonian parameters, including the axial g-tensor ($g_∥$ and $g_⊥$) and hyperfine coupling constants ($A_∥$ and $A_⊥$), were calculated from the spectra. The observed values of $g_∥ > g_⊥$ and $A_∥ > A_⊥$ suggested that the complexes possessed a ($d_{x^2-y^2}$) ground state, consistent with octahedral geometry (Table-1). The exchange interaction between multiple metal centers in the complexes was evaluated using the geometric parameter G, which was calculated using the following equation:

$$G = \frac{(g_∥ - 2)}{(g_⊥ - 2)}$$

Based on previous reports, a G value greater than 4 indicated parallel or slightly misaligned local tetragonal axes, while a G value less than 4 suggested significant exchange coupling interaction and considerable deviation. The experimental G values of the metal complexes studied in this work fall within the range of 4.1-5.2, suggesting the minimal exchange interaction due to their monomeric nature and parallel or slightly misaligned local tetragonal axes [37,38]. For the synthesized complexes in this study, the $g_∥/A_∥$ values ranged from 144 to 165, indicating an octahedral geometry with mild distortion [39,40].

Complex	g-tensor			A × 10⁻⁴ (cm⁻¹)			G
	$g_∥$	$g_⊥$	g_{iso}	$A_∥$	$A_⊥$	A_{iso}	
Cu(II)	2.36	2.07	2.19	165	68	88	5.1
Co(II)	2.31	2.06	2.20	145	66	86	4.4
Ni(II)	2.18	2.04	2.18	147	74	97	4.2

TABLE-1
THE SPIN HAMILTONIAN PARAMETERS OF THE Cu(II) COMPLEX IN DMSO SOLUTION AT LNT

XRD studies: The X-ray diffraction (XRD) patterns of Schiff base ligand, Cu(II) and Ni(II) metal compounds (Fig. 6) indicates that the compounds are crystalline in nature. Using Scherrer's formula, the average crystal sizes of the complexes copper, cobalt, nickel and zinc were found to have crystal diameters of 67, 54, 48 and 76 nm, respectively.

SEM images and EDX mapping: The morphologies of flake, brick, spherical, plate and ball-like structures were observed in the SEM images of the Cu(II), Co(II), Ni(II), and Zn(II) complexes, respectively as shown in Fig. 7. The Schiff base had an average particle size of 61 nm, while the copper, cobalt, nickel, and zinc complexes displayed average particle sizes of 84, 86, 78, and 69 nm, respectively. The purity and the chemical composition of the material was analyzed using EDAX.

Colour mapping visualizations confirmed the presence of metals and elements, including C, N, O, and Cl, which are consistent with the proposed structures of the synthesized compounds.

Biological assessments

DNA interaction (electronic absorption studies): The shifts in the absorption peak to shorter (hypochromic) or longer (bathochromic) wavelengths indicated structural modifications in the DNA [41]. During intercalation with DNA, the stacking interactions occurred between the aromatic chromophore and nucleic acid base pairs. The aromatic chromophore and DNA base pairs engage in a strong π-π* stacking contact during intercalation, a chemical binding process that usually results in hypochromism or bathochromism [42]. The strength of intercalation was related to the degree of hypochromism observed.
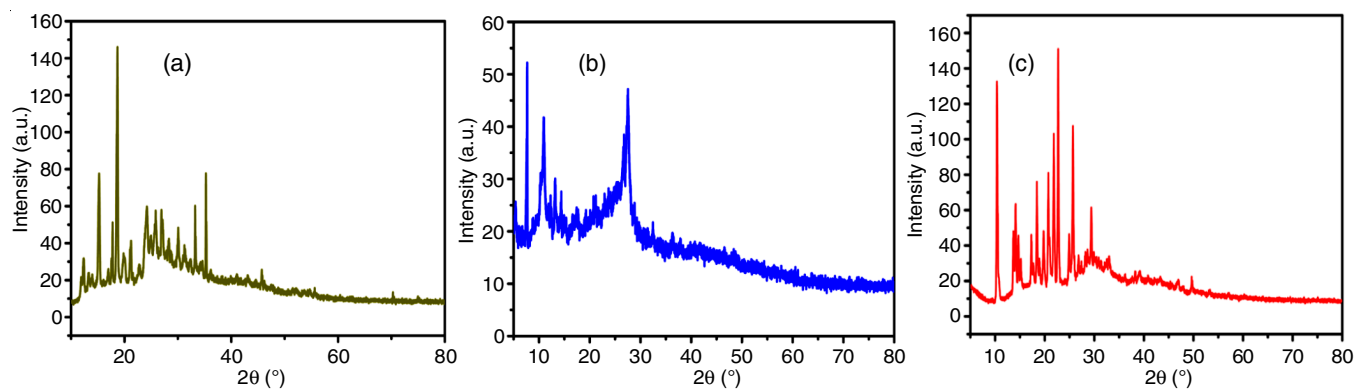

Fig. 6. Powder XRD pattern of (a) Schiff base ligand, (b) Cu(II) complex and (c) Zn(II) complex
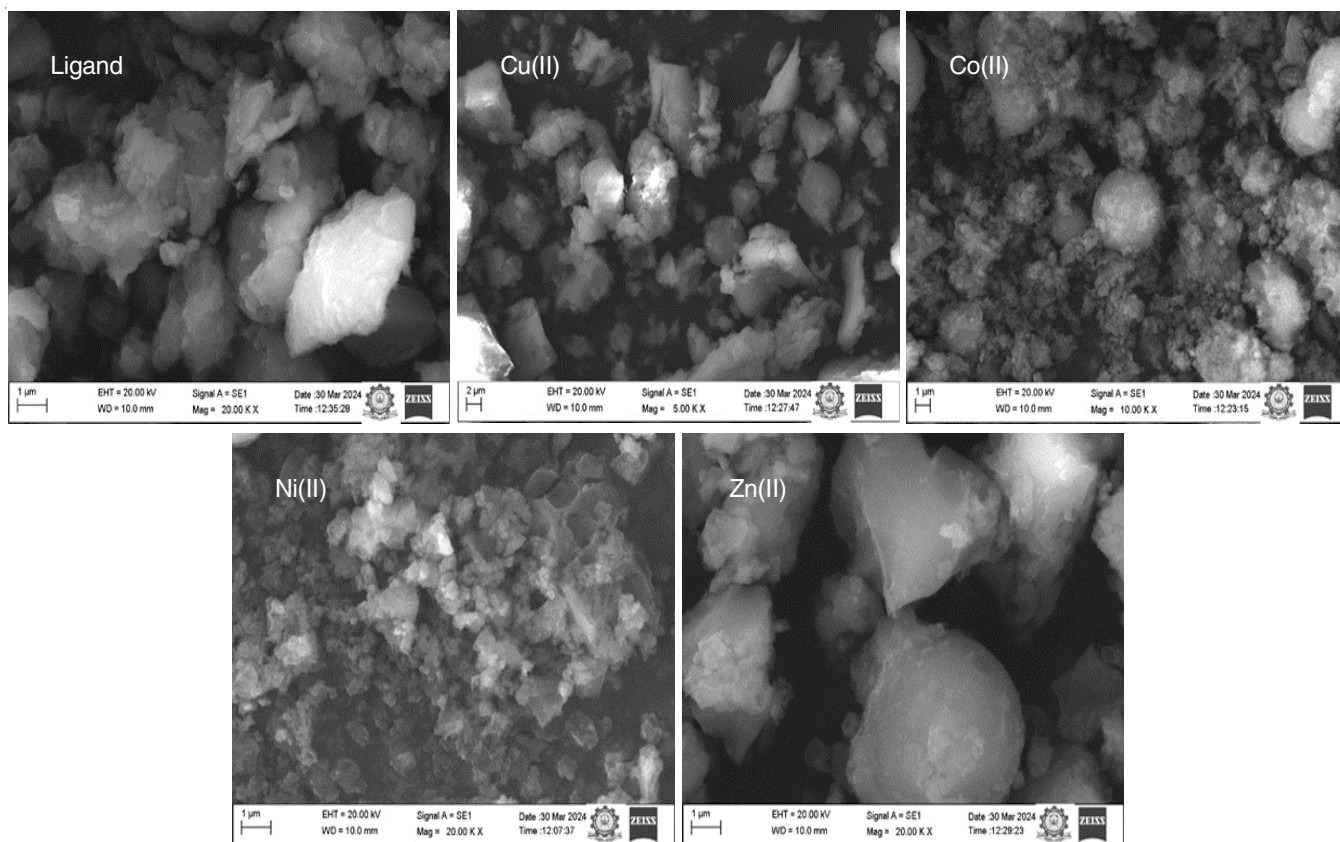

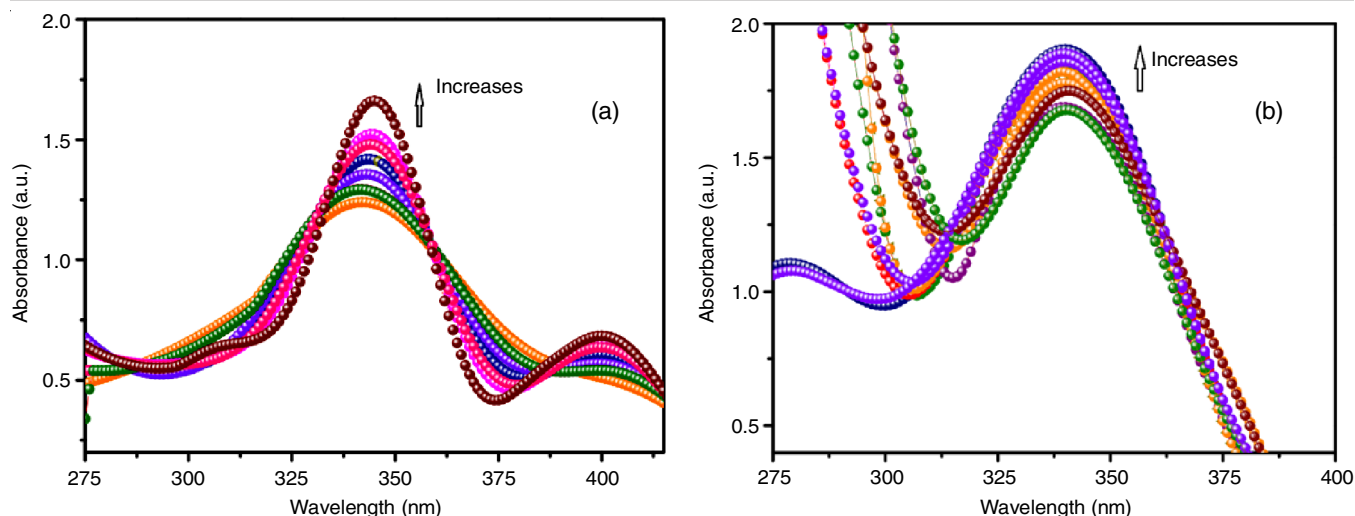Fig. 7. SEM images of the synthesized compounds

Fig. 8. The electronic absorption spectrum of (a) Schiff base ligand and (b) Cu(II) in 5 mM Tris-HCl/50 mM NaCl buffer (pH = 7.2 at 298 K) in the presence of increasing amount of CT-DNA

The interaction of the metal complex with DNA altered its three-dimensional structure, resulting in localized bending and separation. These deformations had the potential to hinder cellular functions such as transcription and DNA replication. The ability of complexes to disrupt double-stranded DNA caused substantial hypochromism, ranging from 10 to 25%. When compounds were inserted between nucleotide base pairs, the π-π* transition of the aromatic group induced a bathochromic shift, with a slight red shift from the original wavelength in the 310-330 nm range.

The binding constant value (K_b) indicated that metal complexes had a higher affinity for DNA than the Schiff base. Due to its small size, ionic radius, positive charge and the presence of heterocyclic co-ligand (1,10-phenanthroline), Cu(II) displayed the highest binding potential (7.8×10^5 M^{-1}) among the complexes. This contributed to enhanced solubility, facilitated absorption into cells *via* active transport and a strong affinity for DNA [43]. This approach demonstrated that these mixed ligand complexes interacted with nucleic acids through an intercalative mode (Table-2). The DNA binding of the ligand and Cu(II) complex are illustrated in Fig. 8.

Hydrodynamic studies: In conventional intercalation, the DNA strand was lengthened and its viscosity increased due to the binding of the synthesized compound to *ct*-DNA base pairs [44]. Since the DNA helix was either stretched or twisted when binding was inconsistent or just partially intercalative, its effective length was reduced and viscosity was decreased. In contrast, the non-intercalative binding, such as groove or electrostatic

interactions, had a minimal effect on viscosity. These results indicated that all complexes are capable of intercalating with nucleotides, as evidenced by the increased viscosity values shown in Fig. 9.
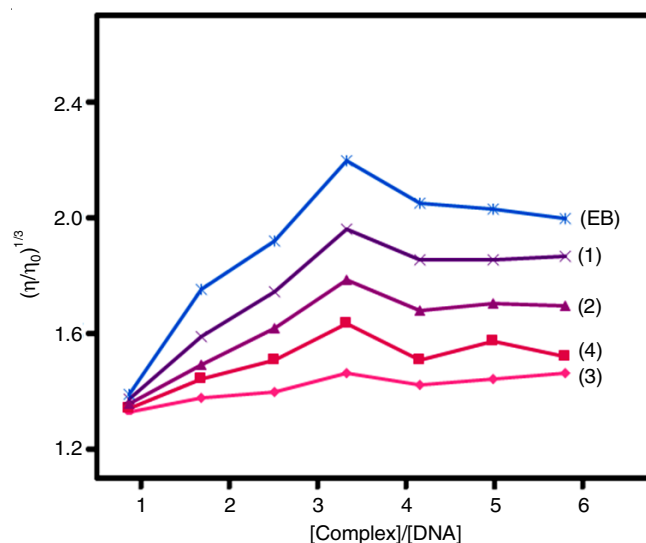
Fig. 9. Effects of increasing amount of classical intercalator [EB] and metal complexes on the relative viscosity of CT-DNA in 5 mmol Tris-HCl/50 mmol NaCl buffer at room temperature, where (1) Cu(II), (2) Co(II), (3) Ni(II) and (4) Zn(II) complexes

DNA chasm: Gel electrophoresis was performed using supercoiled (SC) PBR 322 DNA as substrate and H$_2$O$_2$ to inves-

TABLE-2
ELECTRONIC ABSORPTION PARAMETERS FOR THE INTERACTION OF DNA WITH SYNTHESIZED COMPOUNDS

| Complex | λ_{max} | | $\Delta\lambda$ (nm) | [a]H% | K_b (M^{-1}) |
	Free	Bound			
Ligand	313	316	3	12.5	4.7×10^4
Cu(II)	333	340	7	26.5	7.8×10^5
Co(II)	341	345	4	24.5	7.4×10^5
Ni(II)	342	347	5	23.3	7.2×10^5
Zn(II)	340	344	4	20.6	6.9×10^5

tigate the DNA nuclease activity of the synthesized mixed ligand metal complexes. In DNA electrophoresis, the SC form I of circular plasmid DNA migrated quickly. If a break occurred, the SC form relaxed, resulting in a nicked form that appeared as a slower-moving open circular form II. If both DNA strands were cleaved, a linear form III, migrating between forms I and II, was observed.

Using this oxidative method, the DNA cleavage ability of complexes Cu(II) (lane 3), Co(II) (lane 4), Ni(II) (lane 5), and Zn(II) (lane 6) was demonstrated, converting the DNA to the nicked form, as shown in Fig. 10. In contrast, the control (lane 1), DNA + H_2O_2 (lane 2) and the ligand did not show significant cleavage of plasmid DNA. The cleavage activity was mediated by a metal complex-bound hydroxyl radical species generated by H_2O_2, which broke the phosphodiester backbone through a series of elimination reactions, targeting the C-1 hydrogen of the deoxyribose moiety *via* oxidation [45]. The results indicated that Cu(II) exhibited a higher cleavage capacity, consistent with previous biological findings.
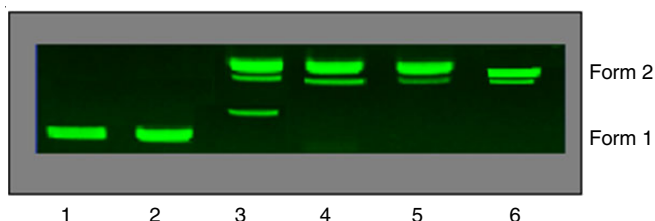

Fig. 10. DNA cleavage of the synthesized compounds in the presence of H_2O_2. Lane 1: DNA + Control; Lane 2: DNA + Ligand; Lane 3: DNA + Cu(II); Lane 4: DNA + Co(II); Lane 5: DNA + Ni(II); Lane 6:DNA + Zn(II)

Antimicrobial activity: The antimicrobial efficacy was evaluated against various microbes using the broth microdilution method. Streptomycin and nystatin were used as reference standards for antibacterial and antifungal activity, respectively. Tables 3 and 4 summarized the antibacterial and antifungal activities of all the synthesized compounds. Among the synthesized complexes, the Cu(II) complex demonstrated comparable antibacterial activity to the standard drug streptomycin, with MIC values ranging from 4.2 to 5.8×10^4 μM compared to streptomycin's MIC values of 2.8 to 3.6×10^4 μM. However, Cu(II) complex exhibited slightly lower antifungal activity than the standard drug nystatin, with MIC values ranging from 9.1 to 9.8×10^4 μM compared to Nystatin's MIC values of 4.2 to 5.1×10^4 μM. The variation in the activity of metal complexes was influenced by factors such as the permeability of the cell membrane and differences in ribosome structure among microbial cells. The lipid bilayer surrounding the cell facilitated the entry of lipid soluble compounds, suggesting that liposolubility was a crucial factor in determining the antimicrobial activity.

Anticancer studies: The synthesized mixed ligand metal complexes were evaluated for their *in vitro* anticancer activity against three different cell lines *viz.* breast cancer (MCF-7), liver cancer (Hep G2), and normal (HBL-100) cell lines. A calorimetric assay with cisplatin as control was used to assess the activity of these complexes. The aforementioned cell lines were treated with mixed ligand complexes at various concentrations for two days. The calorimetric assay (MTT assay) is based on the principle that only living cells are converted to yellow MTT, while non-living cells produce blue formazan products. The results demonstrated that the synthesized mixed ligand complexes inhibited the growth of tumor cells more effectively than the individual complexes or ligands [46]. The ligand exhibited high IC_{50} values of 22 and 20 μM against MCF-7 (breast cancer cells) and Hep G2 (liver cancer cells), respectively. Therefore, free Schiff base was found to be a weak anticancer agent. The mixed ligand complexes exhibited low IC_{50} values indicating their potent anticancer activity. The enhanced anticancer activity may be attributed to chelation, the planarity of two phenanthroline moieties, the size and positive charge of metal, which increased the acidic character of the chelated compound containing protons and facilitated strong hydrogen bonding, thereby amp-

TABLE-3
MINIMUM INHIBITORY CONCENTRATION OF THE SYNTHESIZED COMPOUNDS AGAINST THE GROWTH OF BACTERIA (μM)

Compound	MIC values ($\times 10^4$ μM) SEM = ± 1.5				
	Staphylococcus aureus	*Bacillus subtilis*	*Escherichia coli*	*Klebsiella pneumoniae*	*Salmonella typhi*
Ligand	14.2	15.5	12.8	12.6	13.9
Cu(II)	4.6	4.4	4.8	4.2	5.8
Co(II)	6.3	6.2	6.6	6.7	7.6
Ni(II)	6.9	6.8	7.2	7.6	7.9
Zn(II)	7.7	6.5	6.9	7.2	8.5
Streptomycin	3.5	2.8	2.9	3.5	3.6

TABLE-4
MINIMUM INHIBITORY CONCENTRATION OF THE SYNTHESIZED COMPOUNDS AGAINST THE GROWTH OF FUNGI (μM)

Compound	MIC values ($\times 10^4$ μM) SEM = ± 1.3				
	Aspergillus niger	*Fusarium solani*	*Curvularia lunata*	*Rhizoctonia bataticola*	*Candida albicans*
Ligand	15.5	13.4	12.5	14.8	15.2
Cu(II)	9.8	9.6	9.4	9.2	9.1
Co(II)	11.5	11.6	11.8	12.5	12.3
Ni(II)	12.8	12.6	12.9	13.1	13.5
Zn(II)	9.4	9.7	9.9	9.6	10.5
Nystatin	4.8	4.2	4.6	4.9	5.1

lifying the biological potential of compound. Table-5 clearly demonstrated that Cu(II) exhibited greater anticancer activity than other synthesized metal complexes and the Schiff base ligand.

TABLE-5
THE CYTOTOXIC ACTIVITY OF THE SYNTHESIZED COMPOUNDS AGAINST VARIOUS HUMAN CELL LINES

Compound	IC_{50} values (?M)		
	MCF-7	HepG 2	HBL-100
Ligand	22 ± 0.3	20 ± 0.2	84 ± 0.3
Cu(II)	15 ± 0.4	17 ± 0.2	81 ± 0.5
Co(II)	17 ± 0.5	19 ± 0.2	83 ± 0.8
Ni(II)	19 ± 0.2	20 ± 0.5	86 ± 0.3
Zn(II)	21 ± 0.2	23 ± 0.2	88 ± 0.3
Cisplatin	16 ± 0.1	18 ± 0.6	75 ± 0.4

Antioxidant activity: Using ascorbic acid (vitamin c) as the standard, the DPPH assay was used to carry out the experiment. It was found that the synthesized mixed ligand metal complexes exhibited superior scavenging abilities as a result of chelation in comparison to the free Schiff base (Table-6). Moreover, the antioxidant properties of the metal complexes expand their ability to safeguard organisms against various diseases.

Computational studies

PASS biological activity prediction: The biological activity of Schiff base ligand was determined using the PASS online program. Based on the biological activity predictions, the synthesized Schiff base ligand exhibited the strongest antiviral, antimycobacterial, anti-helmintic, antineoplastic and antileprosy activities (Table-7). It also showed potential as a urokinase inhibitor and lysase inhibitor and demonstrated activity against pancreatic cancer, mucositis and prion diseases.

***In silico* ADMET prediction:** SwissADME software was employed to calculate the bioactive score values of the synthesized compounds, while toxicity parameters were determined using AdmetSAR software. Various parameters including Mi log P (partition coefficient), compound weight, heavy atoms, hydrogen donors, hydrogen acceptors, and rotatable bonds, were estimated. *In silico* ADMET, which encompasses the properties of absorption, distribution, metabolism, excretion and toxicity, was utilized to predict the drug-likeness behaviour of the compounds based on Lipinski's rule of five (Table-8) [47].

Log P: In this study, the Mi Log P values for the synthesized Schiff base ligand and its mixed ligand complexes were found to be less than 5, indicating that these compounds likely possess sufficient permeability to cross the central nervous system. Additionally, the molecular weights of the synthesized

TABLE-7
PASS BIOLOGICAL ACTIVITY SPECTRUM OF SCHIFF BASE LIGAND

Pa	Pi	Activity
0,479	0,003	Urokinase inhibitor
0,533	0,057	Lysase inhibitor
0,486	0,012	Antiprotozoal (Amoeba)
0,452	0,030	Antiinfective
0,445	0,024	Glycerol-3-phosphate dehydrogenase inhibitor
0,443	0,023	Salicylate 1-monooxygenase inhibitor
0,424	0,008	Phenol 2-monooxygenase inhibitor
0,419	0,015	Antiprotozoal (Coccidial)
0,377	0,008	Antihelmintic (Fasciola)
0,469	0,127	Chymosin inhibitor
0,408	0,091	Antiseborrheic
0,393	0,077	Platelet derived growth factor receptor kinase inhibitor
0,343	0,047	Prion diseases treatment
0,294	0,032	Antiprotozoal (Trichomonas)
0,269	0,044	Antiseptic
0,269	0,050	Antihelmintic
0,264	0,069	Antiparasitic
0,284	0,091	Antimycobacterial
0,257	0,066	Uroporphyrinogen-III synthase inhibitor
0,331	0,140	Apyrase inhibitor
0,379	0,188	Pseudolysin inhibitor
0,300	0,110	Glucose oxidase inhibitor
0,279	0,090	DNA polymerase I inhibitor
0,207	0,026	Catalase stimulant
0,247	0,067	Lactose synthase inhibitor
0,341	0,169	Antiviral (Picornavirus)
0,236	0,086	Cell wall biosynthesis inhibitor
0,272	0,138	Antihelmintic (Nematodes)
0,264	0,217	Mucositis treatment
0,185	0,150	Endothelial growth factor antagonist
0,195	0,164	Angiogenesis stimulant
0,191	0,174	Antiviral (Poxvirus)
0,122	0,119	Nuclease inhibitor
0,197	0,194	Antineoplastic (pancreatic cancer)
0,056	0,055	Bcl-xL inhibitor
0,078	0,077	Astringent

where Pa = Probability of active; Pi = Probability inactive

compounds were below 500, aligning with Lipinski's rule of five, suggesting that the compounds meet the criteria for favourable drug-like properties.

H-releasing and withdrawing capacity: It was observed that the Schiff base ligand contained one hydrogen donor and five hydrogen acceptors. However, the metal complexes exhibited twelve hydrogen acceptors and no hydrogen donors. Based on these characteristics, the compounds showed a high number of hydrogen donors and acceptors, which likely contributed to their flexibility and enhanced ability to interact effectively with active sites.

TABLE-6
PERCENTAGE OF ANTIOXIDANT ACTIVITY OF THE SYNTHESIZED COMPOUNDS

Concentration (µg/mL)	Radical scavenging efficiency (%)					
	Ligand	Cu(II)	Co(II)	Ni(II)	Zn(II)	Vitamin c
10	23.40	73.41	32.11	64.8	41.56	80.15
20	26.73	82.32	69.4	74.2	59.12	86.42
30	35.51	87.11	71.8	87.5	62.34	92.36
40	40.8	90.11	82.9	93.1	83.52	95.78

TABLE-8
PREDICTION OF *in silico* ADMET PROPERTIES OF THE SYNTHESIZED COMPOUNDS

| Compounds | m.f. | m.w. (g/mol) | Physico-chemical Parameters | | | | | Bioactivity score | Toxicity parameters |
			log P	TPSA (Å^2)	No. of H bond acceptor	No. of H bond donor	No. of rotatable bonds		Carcinogenic activity/mutagenic activity/irritant
Ligand	$C_{12}H_8N_3O_3Cl$	277	1.40	91.30	5	1	2	0.55	None
Cu(II)	$C_{36}H_{22}N_8O_6Cl_2Cu$	797	1.64	186.38	12	0	8	0.55	None
Co(II)	$C_{36}H_{22}N_8O_6Cl_2Co$	792	1.64	186.38	12	0	8	0.55	None
Ni(II)	$C_{36}H_{22}N_8O_6Cl_2Ni$	792	1.64	186.38	12	0	8	0.55	None
Zn(II)	$C_{36}H_{22}N_8O_6Cl_2Zn$	798	1.64	186.38	12	0	8	0.55	None

TPSA: TPSA was calculated by summing the contributions of O, N and their attached H atoms in the synthesized compounds. This parameter was critical for assessing passive diffusion across cell membranes, supporting the potential of these drug candidates to cross into the central nervous system. In this study, the Schiff base ligand showed a TPSA value of 91.30 Å (below the 140 Å threshold), while the metal complexes had a TPSA of 186.38 Å, indicating that the synthesized compounds exhibit favourable drug transport characteristics and could be suitable for oral administration.

Rotatable bonds: According to Lipinski's rule, an increase in the rotatable bonds enhances the molecular flexibility, allowing better interaction with specific active centers. In this investigation, the synthesized Schff base ligand and the mixed ligand metal chelates were found to have five and two rotatable bonds, respectively. The data indicated that these synthesized compounds possess suitable properties for efficient interaction with living cells.

Bioactivity score prediction: The bioactivity score was assessed by evaluating activity levels as a GPCR ligand, ion channel modulator, nuclear receptor ligand, kinase inhibitor, protease inhibitor, and enzyme inhibitor. In this work, both the Schif base ligand and the mixed ligand metal complexes had a bioactivity score of 0.55. Based on Lipinski's rule, compounds with bioactivity scores exceeding 0 demonstrate strong potential for drug-like characteristics and the results presented here are consistent with this standard.

Toxicity assessment: Mutagenic and carcinogenic activities were analyzed using AdmetSAR software. Toxicity assessment is a key factor in developing novel therapeutic drugs. Based on theoretical results, the synthesized compounds present no toxicity risk.

Conclusion

An novel heterocyclic Schiff base and its mixed ligand metal complexes with enhanced pharmacological properties were synthesized and characterized through various spectral investigations, which revealed that the synthesized complexes had an octahedral structure. Ultraviolet spectroscopy and viscosity measurements conducted during intercalation confirmed the mode of interaction with DNA. Moreover, the DNA cleavage experiment revealed the efficacy of the compounds in cleaving nucleotides. The screening investigation against bacteria indicated that the mixed ligand metal complexes were more effective anti-pathogenic agents than the Schiff base ligand. The presence of a heterocyclic ligand was found to be essential for enhancing the anticancer potential and radical scavenging ability of the synthesized compounds. *In silico* ADMET studies demonstrated the higher biological potential of both the Schiff base ligand and the mixed ligands metal complexes. The substance activity spectrum prediction (PASS) for the synthetic ligand provided evidence of the compound's drug-like properties. The biological investigations indicated that while all the compounds exhibited biological effects, the Cu(II) complex was more potent than the others.

CONFLICT OF INTEREST

The authors declare that there is no conflict of interests regarding the publication of this article.

REFERENCES

1. U. Ndagi, N. Mhlongo and M.E. Soliman, *Drug Des. Devel. Ther.*, **11**, 599 (2017);
https://doi.org/10.2147/DDDT.S119488

2. R.L. Lucaciu, A.C. Hangan, B. Sevastre and L.S. Oprean, Molecules. 27, 6485 (2022);
https://doi.org/10.3390/molecules27196485

3. U. Anand, A. Dey, A.K.S. Chandel, R. Sanyal, A. Mishra, D.K. Pandey, V. De Falco, A. Upadhyay, R. Kandimalla, A. Chaudhary, J.K. Dhanjal, S. Dewanjee, J. Vallamkondu and J.M. Pérez de la Lastra, *Genes Dis.*, **10**, 1367 (2023);
https://doi.org/10.1016/j.gendis.2022.02.007

4. N.J. Wheate, S. Walker, G.E. Craig and R. Oun, *Dalton Trans.*, **39**, 8113 (2010);
https://doi.org/10.1039/c0dt00292e

5. S. Rottenberg, C. Disler and P. Perego, *Nat. Rev. Cancer*, **21**, 37 (2021);
https://doi.org/10.1038/s41568-020-00308-y

6. S.J. Tan, Y.K. Yan, P.P.F. Lee and K.H. Lim, *Future Med. Chem.*, **2**, 1591 (2010);
https://doi.org/10.4155/fmc.10.234

7. C. Marzano, M. Pellei, F. Tisato and C. Santini, *Anticancer. Agents Med. Chem.*, **9**, 185 (2009);
https://doi.org/10.2174/187152009787313837

8. I. Romero-Canelon and P.J. Sadler, *Inorg. Chem.*, **52**, 12276 (2013);
https://doi.org/10.1021/ic400835n

9. I.A. Khan, M.V. Kulkarni, M. Gopal, M.S. Shahabuddin and C.M. Sun, *Bioorg. Med. Chem. Lett.*, **15**, 3584 (2005);
https://doi.org/10.1016/j.bmcl.2005.05.063

10. D. HaMai, S.C. Bondy, A. Becaria and A. Campbell, *Curr. Top. Med. Chem.*, **1**, 541 (2001);
https://doi.org/10.2174/1568026013394796

11. R.K. Mohapatra, P.K. Das, M.K. Pradhan, M.M. El-Ajaily, D. Das, H.F. Salem, U. Mahanta, G. Badhei, P.K. Parhi, A.A. Maihub and M.K. E-Zahan, *Comments Inorg. Chem.*, **39**, 127 (2019); https://doi.org/10.1080/02603594.2019.1594204

12. S. Pullen and G.H. Clever, *Acc. Chem. Res.*, **51**, 3052 (2018); https://doi.org/10.1021/acs.accounts.8b00415

13. S.K. Singh, S. Joshi A.R. Singh J.K. Saxena and D.S. Pandey, *Inorg. Chem.*, **46**, 10869 (2007); https://doi.org/10.1021/ic700885m

14. Y. Li, G. Zhang and M. Tao, *J. Photochem. Photobiol. B*, **138**, 109 (2014); https://doi.org/10.1016/j.jphotobiol.2014.05.011

15. A.K. Sadana, Y. Mirza, K.R. Aneja and O. Prakash, *Eur. J. Med. Chem.*, **38**, 533 (2003); https://doi.org/10.1016/s0223-5234(03)00061-8

16. M. Chauhan, K. Banerjee and F. Arjmand, *Inorg. Chem.*, **46**, 3072 (2007); https://doi.org/10.1021/ic061753a

17. N. Udilova, A.V. Kozlov, W. Bieberschulte, K. Frei, K. Ehrenberger and H. Nohl, *Biochem. Pharm.*, **65**, 59 (2003); https://doi.org/10.1016/S0006-2952(02)01452-1

18. M. Sonmez, M. Celebi and I. Berber, *Eur. J. Med. Chem.*, **45**, 1935 (2010); https://doi.org/10.1016/j.ejmech.2010.01.035

19. A.M. Dar, M.A. Khan, S. Mir and M.A. Gatoo, *Pharm. Anal. Acta*, **7**, 464 (2016); https://doi.org/10.4172/2153-2435.1000464

20. E. Oruc, S. Rollas, F. Kandemirili, N. Shvets and A.S. Dimoglo, *J. Med. Chem.*, **47**, 6760 (2004); https://doi.org/10.1021/jm0495632

21. A. Lagunin, D. Filimonov and V. Poroikov, *Curr. Pharm. Des.*, **16**, 1703 (2010); https://doi.org/10.2174/138161210791164063

22. M.D. Segall, A.P. Beresford, J.M.R. Gola, D. Hawksley and M.H. Tarbit, *Expert. Opin. Drug. Metab. Toxicol.*, **2**, 325 (2006); https://doi.org/10.1517/17425255.2.2.325

23. B. Mathew, J. Suresh, S. Anbazhagan and S. Dev, *Biomed. Aging. Pathol.*, **4**, 327 (2014); https://doi.org/10.1016/j.biomag.2014.07.011

24. T. Sander, J. Freyss, M.V. Korff, J.R. Reich and C. Rufener, *J. Chem. Inf. Model.*, **49**, 232 (2009); https://doi.org/10.1021/ci800305f

25. F. Liu and B.-S. Fang, *Chin. J. Biotechnol.*, **23**, 133 (2007); https://doi.org/10.1016/S1872-2075(07)60012-0

26. A.Z. El-Sonbati, M.A. Diab, A.A. El-Bindary, M.I. Abou-Dobara and H.A. Seyam, *Spectrochim. Acta A Mol. Biomol. Spectrosc.*, **104**, 213 (2013); https://doi.org/10.1016/j.saa.2012.11.024

27. O. Ozdemir, *J. Photochem. Photobiol. Chem.*, **392**, 112356 (2020); https://doi.org/10.1016/j.jphotochem.2020.112356

28. S. Nakamura, R. Nagao, R. Takahashi and T. Noguchi, *Biochemistry*, **53**, 3131 (2014); https://doi.org/10.1021/bi500237y

29. C.X. Wang, Y.H. Yang and G.W. Yang, *J. Appl. Phys.*, **97**, 066104 (2005); https://doi.org/10.1063/1.1863415

30. A.Z. El-Sonbati, W.H. Mahmoud, G.G. Mohamed, M.A. Diab, S.M. Morgan and S.Y. Abbas, *Appl. Organomet. Chem.*, **33**, 5048 (2019); https://doi.org/10.1002/aoc.5048

31. M.I. Khan, A. Khan, I. Hussain, M.A. Khan, S. Gul, M. Iqbal, Inayat-Ur-Rahman and F. Khuda, *Inorg. Chem. Commun.*, **35**, 104 (2013); https://doi.org/10.1016/j.inoche.2013.06.014

32. G.G. Mohamed, *Spectrochim. Acta A Mol. Biomol. Spectrosc.*, **64**, 188 (2006); https://doi.org/10.1016/j.saa.2005.05.044

33. M. Almasi, M. Vilkova and J. Bednarcik, *Inorg. Chim. Acta*, **515**, 120064 (2021); https://doi.org/10.1016/j.ica.2020.120064

34. I. El Heda, J. Massoudi, R. Dhahri, E. Dhahri, F. Bahri, K. khirouni and B.F.O. Costa, *J. Alloys Compd.*, **931**, 167479 (2023); https://doi.org/10.1016/j.jallcom.2022.167479

35. M. Almasi, M. Vilkova and J. Bednarcik, *Inorg. Chim. Acta*, **515**, 120064 (2021); https://doi.org/10.1016/j.ica.2020.120064

36. D.K. Mishra, U.K. Singha, A. Das, S. Dutta, P. Kar, A. Chakraborty, A. Sen and B. Sinha, *J. Coord. Chem.*, **71**, 2165 (2018); https://doi.org/10.1080/00958972.2018.1476687

37. K. Dyrek and M. Che, *Chem. Rev.*, **97**, 305 (1997); https://doi.org/10.1021/cr950259d

38. A. Das, K. Bhattacharya, L.K. Das, S. Giri and A. Ghosh, *Dalton Trans.*, **47**, 9385 (2018); https://doi.org/10.1039/C8DT01400K

39. J. Ammeter, G. Rist and H.H. Gunthard, *J. Chem. Phys.*, **57**, 3852 (1972); https://doi.org/10.1063/1.1678855

40. A.K. Patel, R.N. Jadeja, R.J. Butcher, M.K. Kesharwani, J. Kastner and M. Muddassir, *Polyhedron*, **195**, 114969 (2021); https://doi.org/10.1016/j.poly.2020.114969

41. N.K. Modukuru, K.J. Snow, B.S. Perrin Jr., A. Bhambhani, M. Duff and C.V. Kumar, *J. Photochem. Photobiol. Chem.*, **177**, 43 (2006); https://doi.org/10.1016/j.jphotochem.2005.05.010

42. N. Kumar, R. Kaushal and P. Awasthi, *J. Mol. Struct.*, **1288**, 135751 (2023); https://doi.org/10.1016/j.molstruc.2023.135751

43. M.A. Olusegun, D. Reddy and D. Jaganyi, *Int. J. Chem. Kinet.*, **52**, 884 (2020); https://doi.org/10.1002/kin.21407

44. M. Tripathi, R. Syed, A. Stalin, A. Malik, R. Pande and A.K. Asatkar, *J. Lumin.*, **36**, 1277 (2021); https://doi.org/10.1002/bio.4054

45. R.R. Joshi and K.N. Ganesh, *Biochem. Biophys. Res. Commun.*, **182**, 588 (1992); https://doi.org/10.1016/0006-291X(92)91773-J

46. A.A. Adeleke, M.S. Islam, K. Olofinsan, V.F. Salau, C. Mocktar and B. Omondi, *New J. Chem.*, **45**, 17827 (2021); https://doi.org/10.1039/D1NJ03231C

47. Y.T. Hussein and Y.H. Azeez, *J. Biomol. Struct. Dyn.*, **41**, 1168 (2023); https://doi.org/10.1080/07391102.2021.2017350